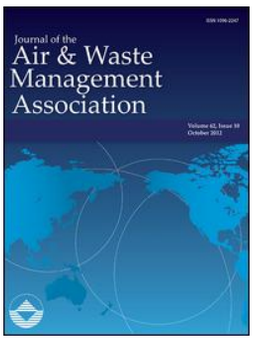

Taylor & Francis
Taylor & Francis Group

Journal of the Air & Waste Management Association

ISSN: 1096-2247 (Print) 2162-2906 (Online) Journal homepage: https://www.tandfonline.com/loi/uawm20

Localizing Gaseous Fugitive Emission Sources by Combining Real-Time Optical Remote Sensing and Wind Data

Ram A. Hashmonay & Michael G. Yost

To cite this article: Ram A. Hashmonay & Michael G. Yost (1999) Localizing Gaseous Fugitive Emission Sources by Combining Real-Time Optical Remote Sensing and Wind Data, Journal of the Air & Waste Management Association, 49:11, 1374-1379, DOI: 10.1080/10473289.1999.10463970

To link to this article: https://doi.org/10.1080/10473289.1999.10463970

TECHNICAL PAPER

ISSN 1047-3289 *J. Air & Waste Manage. Assoc.* **49**:1374-1379

Localizing Gaseous Fugitive Emission Sources by Combining Real-Time Optical Remote Sensing and Wind Data

Ram A. Hashmonay and Michael G. Yost

Department of Environmental Health, University of Washington, Seattle, Washington

ABSTRACT

This paper presents a new approach to localize point emissions from ground-level fugitive gaseous air pollution sources. We estimate the crosswind plume's ground-level peak location downwind from the source by combining smooth basis functions minimization (SBFM) with path-integrated optical remote sensing concentration data acquired along the crosswind direction in alternating beam path lengths. Peak location estimates, in conjunction with real-time measured wind direction data, are used to reconstruct the fugitive source location. We conducted a synthetic data study to evaluate the proposed peak location SBFM reconstruction. Furthermore, the methodology was validated with open-path Fourier transform infrared concentration data collected with wind direction data downwind from a controlled point source. This approach was found to provide reasonable estimates of point source location. The field study reconstructed source location was within several meters of the real source location.

INTRODUCTION

This study applies path-integrated optical remote sensing (PI-ORS), innovative mathematical inversion techniques, and wind data to determine fugitive gaseous air pollution upwind source location. The described methodology is designed to provide an applicable PI-ORS monitoring approach for estimating the emission point source location directly from the measured concentration and wind data, without employing any dispersion model. Furthermore, this study may provide an estimate of the plume's crosswind concentration profiles downwind from the emission source. Along with the importance of identifying the source location for on-site worker's exposure control, these parameters may provide the essential input needed for a dispersion model to produce reliable exposure estimates at downwind neighboring communities.

Previous studies[1-8] have addressed emissions from fugitive sources, such as landfills,[3] coal mines,[5,6] or water treatment plants,[7,8] using PI-ORS technologies. No previous investigations addressed the issue of localizing "hot spots" of emissions. Our earlier studies were focused on combining downwind path integrated concentration (PIC) data, wind measurements, and plume dispersion modeling to roughly spatially apportion the emission rates within the area source boundaries.[9] However, this approach was limited to apportion emissions across the wind direction, and one had to a priori assume the area source location and dimension.

Techniques such as differential absorption lidar (DIAL)[10] and computed tomography using PI-ORS data[11] could be applied to directly measure a spatially resolved map of the contaminant concentrations over the source. The peak location in the measured map may correspond to the source location; however, no information could be retrieved on the emission rate of the identified source. Furthermore, classical computed tomography (CT) geometries are very complex and costly and are not likely to be applied to outdoor measurements.[11]

Recently, our CT efforts have focused on developing an algorithm that will allow reconstruction of a concentration field in a plane, based on non-overlapping PIC data scanned in radial alternating path lengths.[12] The authors and others[12,13] have shown that the smooth basis functions minimization (SBFM) approach[14] can provide the desired field of concentration with a relatively sparse beam geometry. This could have been applied to reconstruct the field of concentration over the emission source area, but would suffer the same disadvantage as the DIAL and previous CT geometries of not being capable

IMPLICATIONS

The suggested technology may provide fairly robust and near real-time estimates of point emission location of various ground-level fugitive sources. This methodology could be applied in conjunction with methodologies for flux estimation, as an alarm for the source's departure from normal working conditions. The estimated source location, along with the estimated flux, could be input into a dispersion model to calculate the downwind field of concentrations.

to estimate the emission rates. Therefore, we suggested[15] applying this innovative SBFM approach to reconstruct the smoothed field of concentration in the downwind vertical plane as was done with DIAL.[10] This allowed us to calculate the plane integrated concentration and thus the emission flux. As shown in Figure 1, we planned the vertical plane beam geometry to include several ground-level beam paths to satisfy the PIC data required for the methodology described in this paper. This will combine the two methodologies into one scanning procedure that will simultaneously provide both the source emission flux and the location.

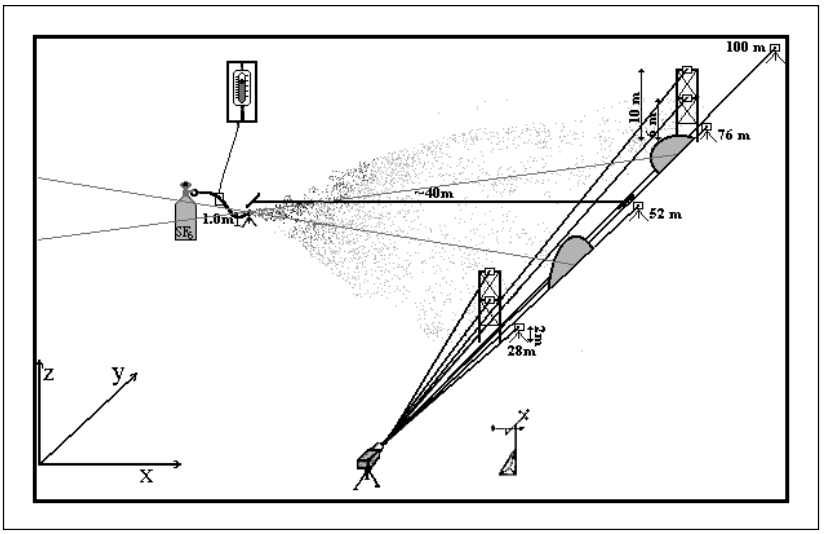

Figure 1. Suggested combined experimental setup for the localization and emission flux method.[15]

METHODOLOGY

A one-dimensional SBFM reconstruction can be applied to the ground-level segmented beam paths (Figure 1) of the same beam geometry to find the crosswind concentration profile.[15] The plume crosswind peak location coupled with the average wind direction data could provide an idea of the emission source location and configuration. As before, a Gaussian function is fitted to measured PIC ground-level values, but this time as a univariate function. The error function for the minimization procedure is the sum of squared errors (SSE) function, and it is defined in the one-dimensional SBFM approach as follows:

$$SSE(B_j, m_{y_j}, \sigma_{y_j}) = \sum_i \left(PIC_i - \sum_j \frac{B_j}{\sqrt{2\pi}\sigma_{y_j}} \int_0^{r_i} \exp\left[-\frac{1}{2} \left(\frac{m_{y_j} - r}{\sigma_{y_j}} \right)^2 \right] dr \right)^2 \quad (1)$$

where B is equal to the area under the Gaussian distribution that is equal to the total path integrated concentration, r_i is the path length of the ith beam, m_y is the mean (peak location), and σ_y is the standard deviation of the jth Gaussian function. PIC_i is the observed path integrated concentration value of the ith path.

This Gaussian approximation to the actual distribution could be obtained by minimizing the SSE function to fit the three unknown parameters for each Gaussian function. Figure 2 presents two examples of an arbitrary distribution along with normal distribution reconstructions in different measurement and procedure conditions. As shown in Figure 2, it appears possible that fitting a Gaussian distribution to a single mode arbitrary distribution provides a reasonable estimate of the distribution center of mass location (peak location) and variability.

Over time, as the wind direction fluctuates, different peak locations are reconstructed from the PIC measurements. Each time a peak location is identified, a source projection line is drawn by calculation of a line equation through the peak location with the same orientation as the wind direction averaged over the same measurement interval. Ideally for a stationary point source, all source projection lines drawn over time should intersect at a point upwind of the measurement line in the vicinity of the real emission source location. In practice, the source projection lines do not always converge to a single point. However, by calculating the density of lines per unit area upwind from the measurement plane, the most likely location of the source can be interpreted as the region of the maximal line density.

Table 1. Summary of averaged CCF (goodness-of-fit measure) and averaged absolute shift in peak location values for the same 100 underlying test distributions in the four cases examined (6 meter plus total path length).

	Four Segments		Three Segments	
	Fitting Two Gaussian Function	Fitting One Gaussian Function	Fitting Two Gaussian Function	Fitting One Gaussian Function
Mean CCF	0.95 ± 0.03	0.92 ± 0.06	0.90 ± 0.08	0.90 ± 0.08
Mean Shift in Peak Location [R.U.]	0.41 ± 0.28	0.43 ± 0.33	0.43 ± 0.31	0.39 ± 0.32

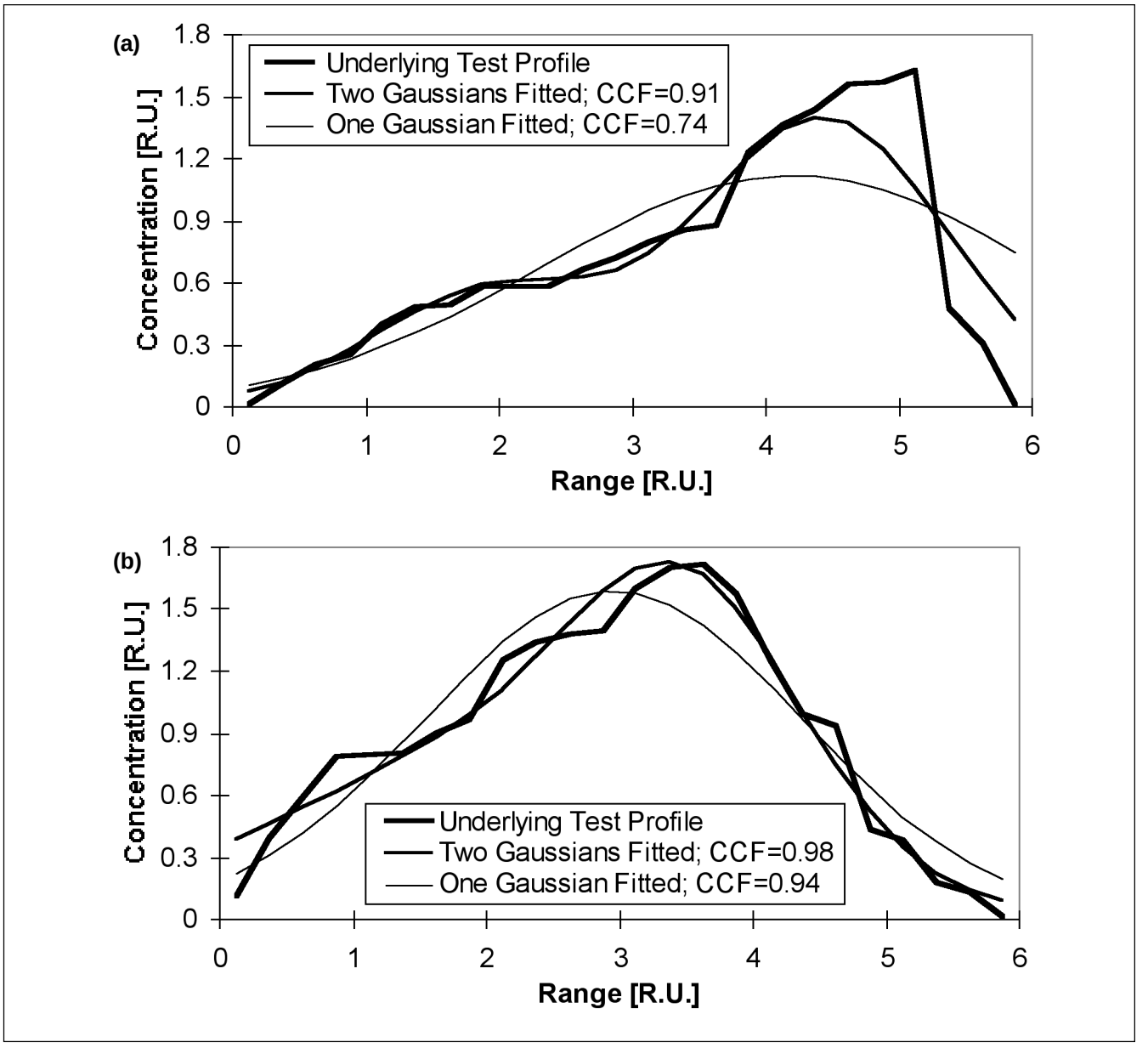

Figure 2. Two examples of reconstructed concentration distributions where one or two Gaussian functions were fitted to four segments of PIC data and CCF values as goodness-of-fit measure: (a) skewed underlying test distribution; (b) approximately symmetric underlying test distribution.

SIMULATION STUDY

The simulated data study was designed to evaluate the number of segments and the number of basis functions needed to accurately estimate the peak location along the primary measurement path. Since each Gaussian distribution has three independent parameters, three segments are sufficient for reconstructing crosswind profiles fitting a single Gaussian. However, when the crosswind profile is nonsymmetric, fitting a single Gaussian function would presumably provide a peak estimated location shifted to the skewed tail of the profile. Since fitting more than one basis function could provide a better fit to a nonsymmetric actual profile, we also fitted two Gaussian functions to evaluate whether we could gain a better estimate of the peak location. In this case, three segments are way underdetermined when searching for six unknown parameters (three for each Gaussian function). Therefore, we compared between three and four segments fitting one or two Gaussian basis functions; a total of four cases, as shown in Table 1. We generated 100 arbitrarily chosen test distributions and performed the SBFM reconstruction procedure for each test distribution in the above four cases.

Each arbitrary test distribution was generated as follows: The computer selected a vector R of 24 uniformly distributed random numbers between 0 and 1. The mode location occurred at the maximal value in this vector. The values prior to the mode were sorted in ascending order

and the values beyond the mode were sorted in descending order to create a single mode distribution. To obtain more peaked test distributions R', the random vector R was modified by the following formula:

$$\vec{R}' = \exp(\vec{R}) - 1 \quad (2)$$

We arbitrarily scaled all of these results to a total path of 6 m; however, any total path could be accommodated in a similar way. The simulated path was equally divided into several (three or four in our simulation) secondary segments. This test distribution was then used to generate synthetic observed PIC data by integrating the random vector values for the relevant secondary path (from the instrument to the relevant simulated retroreflector location). The segmented PIC data were used in the one-dimensional SBFM procedure, minimizing the SSE function to fit the Gaussian distributions to the concentration profile along the main 6-m path.

The concordance correlation factor[16] (CCF) was chosen as a summary measure to represent the quality of the reconstruction fit to the test distribution. This measure was calculated from a linear regression of paired point values taken from the reconstruction and input test distribution at each of the 24 locations along the 6-m path. The CCF is similar to the Pearson correlation coefficient, but is adjusted to account for shifts in location and scale. In our results, the CCF values were only slightly smaller than the Pearson correlation factor. Like the Pearson correlation, CCF values are bounded between -1 and 1, yet the CCF can never exceed the absolute value of the Pearson correlation factor. The CCF will be equal to the Pearson correlation when the linear regression line intersects the ordinate at 0 and its slope equals 1.

For each of the four cases, we averaged the CCF values over the 100 reconstructed test distributions. The results are shown in Table 1, along with the averaged absolute shift in peak location between the test and reconstructed distributions. In addition, all averaged values are presented including the related standard deviations. As can be concluded from Table 1, scanning among four retroreflectors rather than three provides better fits and smaller shifts in peak location. Furthermore, when scanning to four retroreflectors, fitting two Gaussian functions seems beneficial compared to fitting only one. Examples that demonstrate the effects of fitting two Gaussian functions are illustrated in Figure 2. The tail of the skewed test distribution is taken into account in Figure 2a by one of the functions, allowing the other function to better estimate the peak location and to provide an overall better fit. However, note that the difference in estimated peak location is very small. In a more symmetric case (test distribution in Figure 2b), there is a smaller difference between fitting one or two Gaussian functions.

FIELD STUDY

To validate the feasibility of this approach to estimate the point source location, a field experiment was conducted. The general site configuration in the field experiment was described in a previous paper.[9] The source was simulated by a controlled point source of sulfur hexafluoride (SF_6) gas, elevated from the ground by 0.7 m. An open-path Fourier transform infrared (OP-FTIR) (bistatic BOMEM 155MB) beam path was located 40 m downwind from the controlled point source and approximately perpendicular to the average wind direction (Figure 3). The 75-m OP-FTIR beam path was segmented by two additional radiation sources (bistatic) into shorter path lengths of 52 and 32 m. As radiation sources, we used three $1 \times 1 \times 0.2$-m containers of water, electrically heated up to the boiling temperature. The 1-m^2 surface of the radiation source was facing the instrument and was painted in an emissive black paint. As the physical size of the infrared source covers all of the field of view of the collecting optics of the instrument, no background signal acquisition and subtraction were needed in this study. The highest spectral resolution of the BOMEM system is 1 cm^{-1}. The BOMEM instrument includes a Sandwich MCT/InSb cooled detector apparatus; however, since the SF_6 absorbance feature is around 950 cm^{-1}, the data acquisition was performed between 900 and 1000 cm^{-1} in the MCT spectral range.

Meteorological data were acquired by a meteorological station located at the site. This station is 3.5 m above the ground level and provided wind data averaged over 5-min intervals. The wind data were integrated to overlap the measurement time interval, which was typically 20 min. The wind direction sensor was counterbalanced, with lightweight vanes attached to a shaft coupled to a precision low-torque potentiometer. This sensor had a starting threshold of 0.22 m/sec and accuracy of ±2°.

The OP-FTIR instrument continuously sampled for 1 min on each beam segment and consequently acquired data for about 20 min. This yielded at least six repeats on each of the three beam paths. The plume peak location was determined for nine runs using the one-dimensional SBFM method. The average wind direction was measured and coupled with the peak location to calculate the source projection line density function as described in the previous section. The line density function was computed for pixel size of 2×2 m, and a contour map of this function is plotted in Figure 3. The region with the highest line density appears in the map very close to the actual source location (at 0,0 at the contour map in Figure 3). The high density of lines upwind of the source location is probably due to the small variations in wind direction over the experiment. This made the determination of the source location more uncertain along the direction of the average wind direction.

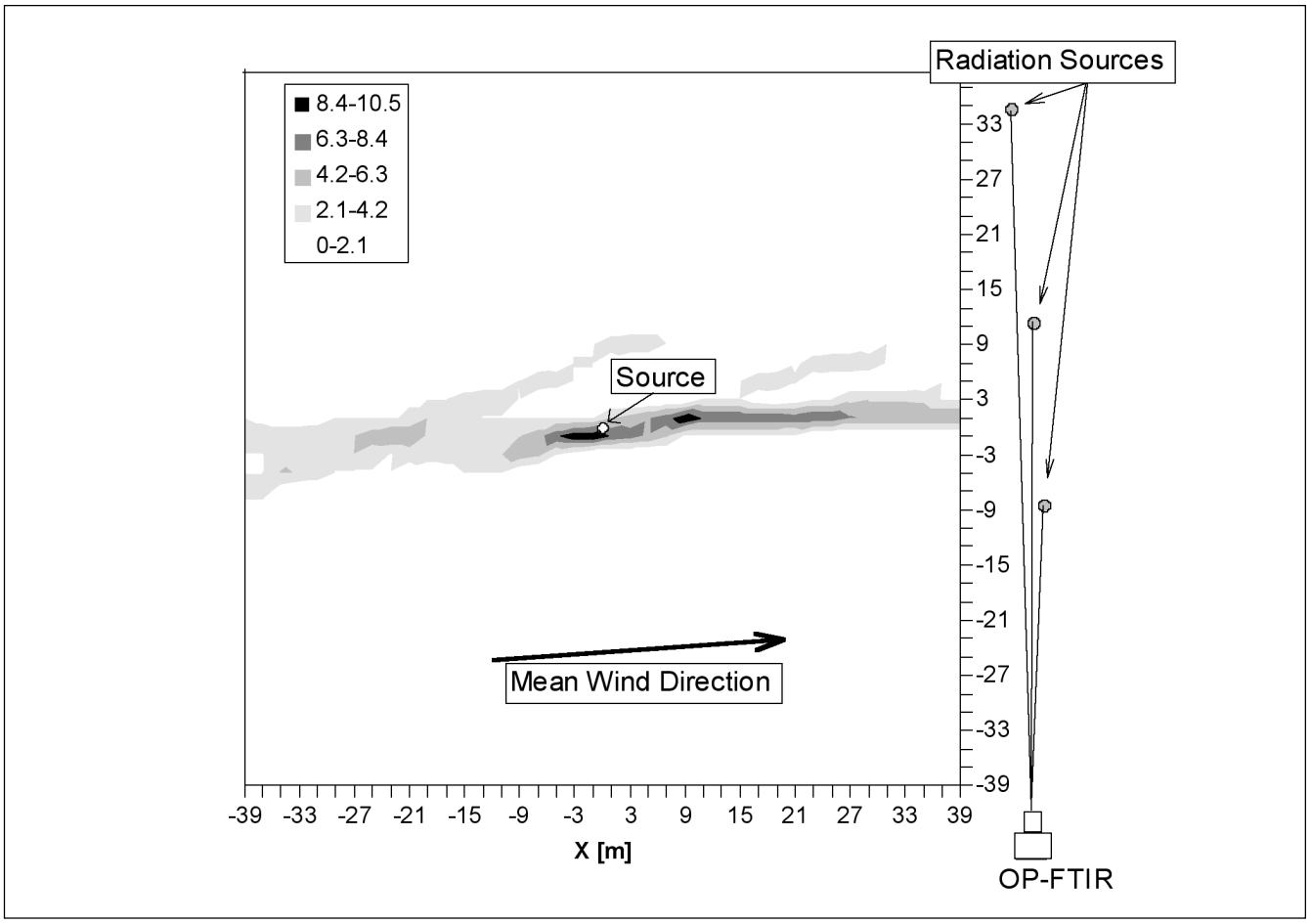

Figure 3. A contour map of the source projection line density function in units of $(2 \times 2 \times m)^{-1}$. The actual point source location is at the origin of the Cartesian coordinate system (0,0), and is indicated by the white circle.

CONCLUSIONS

The one-dimensional SBFM approach was found to be feasible for estimating the crosswind plume's peak location for four cases examined in the simulation study. The four-segment case, where two Gaussian functions were fitted, seemed to provide the best results with regard to overall goodness of fit. However, there is no significant difference in the estimation of peak location. Scanning to three retroreflectors will provide better temporal resolution that may provide a better peak location reconstruction (than the four segments) in real field setup situations. This issue will be explored experimentally in the next phase of this research program.

Furthermore, as was shown with OP-FTIR experimental data (which employed three segments), by combining wind direction data and the one-dimensional SBFM approach, it was possible to estimate the point source location based on the source projection line density function. However, note that this was performed over a period of about 3 hr (nine runs of 20 min). By coupling the emission flux[15] and source localization methodologies, one has to retrieve both estimates in the same time interval of about 20 min. Therefore, it is necessary to first apply the reconstruction algorithm for each round of ground-level segmented beams data. For this purpose, it also essential to investigate the issue of how to consider the time lag of the plume traveling from the source to the downwind measurement beam paths.

In this stage of the study, we have not yet considered the reconstructed crosswind standard deviations. This additional information might improve the localization methodology and provide even better estimates of the area source "hot spot" location.

ACKNOWLEDGMENTS

This research was partially supported by the Consortium for Risk Evaluation with Stakeholder Participation (CRESP) through U.S. Department of Energy (DOE) Cooperative Agreement #DE-FC01-95EW55084. This research also was partially supported by the National Institute for Occupational Safety and Health (NIOSH) grant RO1OH02660. This support does not constitute an endorsement by DOE or NIOSH of the views expressed in this article.

REFERENCES

1. Scotto, R.L.; Minnich, T.R.; Leo, M.R. A Method for Estimating VOC Emission Rates from Area Sources Using Remote Optical Sensing. In *Proceedings of the U.S. Environmental Protection Agency/Air & Waste Management Association International Symposium on the Measurement of Toxic and Related Air Pollution*, Raleigh, NC, 1991; p 698.
2. Minnich, T.R.; Scotto, R.L.; Leo, M.R.; Sanders, B.C.; Perry, S.H.; Pritchett, T.H. A Practical Methodology Using Open-path FTIR Spectroscopy to Generate Gaseous Fugitive-source Emission Factors at Industrial Facilities. In *Proceedings of the SP-81 Optical Remote Sensing, Application to Environmental and Industrial Safety Problems*, Pittsburgh, PA, 1992; p 513.
3. Milton, M.J.T.; Partridge, R.H.; Goody, B.A. Minimum Emission Rates Detectable from Landfill Sites Using Optical Integrated-Path Techniques. In *Proceedings of the Air & Waste Management Association International Specialty Conference on Optical Sensing for Environmental and Process Monitoring*, VIP-55; Air & Waste Management Association: Pittsburgh, PA, 1996; p 393.
4. Piccot, S.D.; Masemore, S.S.; Lewis-Bevan, W.; Ringler, E.S; Harris, D.B. "Field assessment of a new method for estimating emission rates from volume sources using open-path FTIR," *J. Air & Waste Manage. Assoc.* **1996**, *46*, 159.
5. Piccot, S.D.; Masemore, S.S.; Ringler, E.S.; Srinivasan, S.; Kirchgessner, D.A.; Herget, W.F. "Validation of a method for estimating pollution emission rates from area sources using open-path FTIR spectroscopy and dispersion modeling techniques," *J. Air & Waste Manage. Assoc.* **1994**, *44*, 271.
6. Kirchgessner, D.A.; Piccot, S.D.; Chadha, A. "Estimation of methane emissions from a surface coal mine using open path FTIR spectroscopy and modeling techniques," *Chemosphere* **1993**, *26* (1-4), 23.
7. Simpson, O.A.; Kagan, R.H. Measurements of Emissions at a Chemical Waste Water Site With an Open Path Remote Fourier Transform Interferometer. In *Proceedings of the U.S. Environmental Protection Agency/Air & Waste Management Association International Symposium on the Measurement of Toxic and Related Air Pollution*, Raleigh, NC, 1990; p 937.
8. Whitcraft, W.K.; Wood, K.N. Use of Remote Sensing to Measure Wastewater Treatment Plant Emissions. In *Proceedings of the 83rd Annual Meeting and Exhibition of the Air & Waste Management Association*; Air & Waste Management Association: Pittsburgh, PA, 1990.
9. Hashmonay, R.A.; Yost, M.G.; Mamane, Y.; Benayahu, Y. "Emission rate apportionment from fugitive sources using open-path FTIR and mathematical inversion," *Atmos. Environ.* **1999**, *33* (5), 735-743.
10. Weibring, P.; Andersen, M.; Ender, H.; Svanberg, S. "Remote monitoring of industrial emissions by combination of lidar and plume velocity measurements," *Appl. Phys.* **1998**, *66* (3), 383-388.
11. Fischer, M.L.; Drescher, A.C.; Gadgil, A.J.; Yost, M.G. A System for Rapid Detection and Mapping of Gas Plumes on 100-m Scales: Examination of Some Technical and Economic Issues. In *Proceedings of Optical Sensing for Environmental and Process Monitoring*; Air & Waste Management Association and SPIE: McLean, VA, 1994; pp 51-159.
12. Hashmonay, R.A.; Yost, M.G.; Wu, C.F. "Computed tomography of air pollutants using radial scanning path-integrated optical remote sensing," *Atmos. Environ.* **1999**, *33* (2) 267- 274.
13. Price, P.N. "Pollutant tomography using integrated concentration data from non-intersecting optical paths," *Atmos. Environ.* **1999**, *33* (2) 275-280.
14. Drescher, A.C.; Gadgil, A.J.; Price, P.N.; Nazaroff, W.W. "Novel approach for tomographic reconstruction of gas concentration distributions in air: Use of smooth basis functions and simulated annealing," *Atmos. Environ.* **1996**, *30* (6), 929.
15. Hashmonay, R.A.; Yost, M.G. "Innovative approach for estimating gaseous fugitive fluxes using computed tomography and remote optical sensing techniques," *J. Air & Waste Manage. Assoc.* **1999**, *49*, 966-972.
16. Li, L.I. "A concordance correlation coefficient to evaluate reproducibility," *Biometrics* **1989**, *45* (3), 225-268.

About the Authors

Dr. Ram A. Hashmonay, M.S., Sc.D., is a research associate at the University of Washington, Department of Environmental Health, Box 357234, Seattle, WA 98195. Dr. Michael G. Yost, M.S., Ph.D., is an associate professor at the University of Washington, Department of Environmental Health, Industrial Hygiene Program Director, Box 357234, Seattle, WA 98195.